PHYSICAL REVIEW B VOLUME 51, NUMBER 16 15 APRIL 1995-II

Pulse propagation and many-body effects in semiconductor four-wave mixing

A. Schulze, A. Knorr, and S.W. Koch
Fachbereich Physik und Zentrum für Materialwissenschaften, Philipps-Universität, Renthof 5, D-35032 Marburg, Germany
(Received 27 April 1994; revised manuscript received 23 December 1994)

The semiconductor Maxwell-Bloch equations are solved to study the simultaneous influence of pulse propagation effects and Coulomb many-body interaction on the four-wave-mixing signal of semiconductors. Temporal and spatial modulations as well as the decay of time-resolved and time-integrated signals are analyzed for various excitation conditions. It is shown that propagation effects may significantly modify the line shapes depending on sample thickness and excitation conditions. In most cases the signal is more influenced by its own propagation than by the propagation of the input pulses. Exciton-polariton effects are recovered in the low intensity limit. For relatively thin samples an increased temporal decay is observed whereas for thicker samples the propagation effects lead to strong beats in real time. For higher intensities, where an echolike structure is generated, the competition of signal generation by the pump pulses and absorption by the semiconductor determines the output.

I. INTRODUCTION

Recently, several experimental and theoretical studies examined the influence of Coulomb many-body effects on the time-resolved and time-integrated four-wave-mixing signals (FWMS) emitted by semiconductor slices.[1–3] It was shown that Coulomb exchange contributions, which are contained in the optical Bloch equations for the semiconductor, cause time delayed components in the time resolved FWMS. Furthermore, it has been predicted that, in contrast to FWM in atomic systems, signals at negative time delays arise as a consequence of the Coulomb many-body interactions among the electronic semiconductor excitations. Most of these results were obtained for thin samples and do not include pulse distortion effects induced by light propagation through the sample.

On the other hand, it was shown that polariton effects in linear pulse propagation lead to significant pulse distortions.[4] These effects have been investigated experimentally measuring time-integrated FWMS. The corresponding experiments have been modelled using coupled Maxwell-Bloch equations where the semiconductor is treated by the two-level atomic dynamics[5] or by reduced semiconductor Bloch equations which include many-body Coulomb interactions only in the so-called local-field approximation.[6] Other investigations, which discuss propagation induced features in FWM followed, see, e.g., Refs. 7 and 8. A general conclusion from the studies including propagation aspects is that under suitable conditions pulse reshaping and propagation induced distortions may contribute to the signal and lead to features which in some aspects resemble the Coulomb induced FWM signatures. For instance, negative time delay signals are observed if the Coulomb many-body effects are neglected but propagation effects of the light pulses in a finite size sample are included in the calculation.[5] In particular it was found that oscillating time integrated signals are induced by polariton formation in thick samples.[5,6,8] From these studies it can be seen that propagation effects may be of great importance under certain experimental conditions.

In extension of the previous studies we discuss in this paper propagation effects in FWMS using the semiconductor Maxwell-Bloch equations (SMBE).[9] The equations consist of (i) a set of reduced wave equations for the different propagation directions of incident and FWMS pulses and (ii) the semiconductor Bloch equations (SBE) which describe the dynamics of the polarization which acts as a source for the field components.[10] This approach allows a simultaneous description of pulse propagation effects and semiconductor many-body effects for various excitation conditions, especially under the condition that the excitation-induced signal is generated. Furthermore we can distinguish FWMS contributions which are generated by pulse propagation from those caused by many-body effects. This topic is especially interesting because the previous studies were restricted either to the full semiconductor Bloch equations neglecting propagation or to a local field model including pulse propagation.

In the present paper we analyze different experimentally relevant conditions, such as resonant excitation of the $1s$ exciton and of the continuum states for a set of different intensities. The signals are investigated as a function of the sample length and we discuss the coupling mechanisms responsible for the observation of the various propagation effects. The paper is organized as follows. In Sec. II we outline the basic equations and discuss the temporal and spatial analysis of FWM configurations. In Sec. III we present numerical results assuming resonant, spectrally sharp low intensity excitation of the $1s$ exciton absorption peak. We analyze the basic mechanism of the observed propagation effects with special emphasis on the dependence of the FWMS on the sample length. In Sec. IV the analysis is done for the excitation of continuum states. The intensity dependence of the FWMS is investigated for different spectral detunings in Sec. V. Our results are summarized in Sec. VI and in Appendix A we

0163-1829/95/51(16)/10601(9)/$06.00

present details of an approximate analytical solution for the FWMS propagation if the excitation takes place at the $1s$ resonance. Appendix B shows that for low intensity excitation at the exciton resonance the previously used local field model yields results in good agreement with the full calculations.

II. BASIC EQUATIONS

To calculate the FWM components of the optical field we start from the scalar wave equation for a planar semiconductor structure:

$$-\frac{\partial^2 E}{\partial^2 z}-\frac{\partial^2 E}{\partial^2 x}+\frac{1}{c^2}\frac{\partial^2 E}{\partial^2 t}=-\mu_0\frac{\partial^2 P_{\mathrm{tot}}}{\partial^2 t}\ , \tag{1}$$

where E is the optical field. Here, the total polarization P_{tot} acts as a source term in the wave equation and has to be extracted from the semiconductor Bloch equations (SBE). The coordinates x, z describe the linear dimension, where L is the thickness of the sample in propagation direction. As usual in a FWM experiment the surface of the sample ($z=0$) is illuminated by two plane wave light pulses with different propagation constants in the x direction:

$$E=\frac{1}{2}e^{+i\omega_L t-ik_z z}[A_{-1}(t,z)e^{-ik_x x}+A_{+1}(t,z)e^{+ik_x x}]\ , \tag{2}$$

where the input pulse shapes $A_1(t,z=0), A_2(t,z=0)$ are known and assumed to have a Gaussian shape. The temporal delay between both pulses is given by τ, where a negative τ implies that the pulse -1 arrives before the pulse $+1$ at the entrance of the sample. We restrict our considerations to a plane wave expansion for the polarization and the optical field:

$$E=\frac{1}{2}\sum_n A_n e^{-ink_x}e^{-ik_z z+i\omega_L t}+\text{c.c.}\ , \tag{3}$$

$$P_{\mathrm{tot}}=\frac{2d}{V}\sum_n P_n e^{-ink_x}e^{-ik_z z+i\omega_L t}+\text{c.c.}\ , \tag{4}$$

where the envelopes A_n, P_n are slowly varying Fourier components in time and space and ω_L is the carrier frequency of the pulses.

The ansatz (4) for the polarization and the optical field is inserted into the wave equation to extract the signal in the four-wave-mixing direction. Neglecting nonresonant terms we obtain a set of equations describing the propagation of the light field envelope A_n in the directions $-k_z z-nk_x x$:

$$\frac{1}{c^2}\frac{\partial^2 A_n}{\partial t^2}-\frac{\partial^2 A_n}{\partial x^2}-\frac{\partial^2 A_n}{\partial z^2}+\frac{2i}{c^2}\omega_L\frac{\partial A_n}{\partial t}+2ink_x\frac{\partial A_n}{\partial x}+2ik_z\frac{\partial A_n}{\partial z}+\left(n^2k_x^2+k_z^2-\frac{\omega_L^2}{c^2}\right)A_n$$

$$=\frac{4\mu_0 d}{V}\left(\omega_L^2 P_n+2i\omega_L\frac{\partial P_n}{\partial t}+\frac{\partial^2 P_n}{\partial t^2}\right). \tag{5}$$

For the incident pulses $n=+1,-1$ the propagation equation reads

$$\frac{1}{2i\omega_L^2}\frac{\partial^2 A_n}{\partial t^2}-\frac{1}{2i}\frac{\partial^2 A_n}{\partial z_n^2}+\frac{\partial A_n}{\partial z_n}+\frac{1}{\omega_L}\frac{\partial A_n}{\partial t}=\frac{-i2\mu_0 d}{V(k_x^2+k_z^2)}\left(\omega_L^2 P_n+2i\omega_L\frac{\partial P_n}{\partial t}+\frac{\partial^2 P_n}{\partial t^2}\right), \tag{6}$$

whereas the equation for the FWMS $n=3$ is given by

$$\frac{1}{2i\omega_L^2}\frac{\partial^2 A_3}{\partial t^2}-\frac{1}{2i}\frac{\partial^2 A_3}{\partial z_3^2}+\frac{\partial A_3}{\partial z_3}+\frac{1}{\omega_L}\frac{\partial A_3}{\partial t}-i4k_x^2/(k_x^2+k_z^2)A_3=\frac{-i2\mu_0 d}{V(k_x^2+k_z^2)}\left(\omega_L^2 P_3+2i\omega_L\frac{\partial P_3}{\partial t}+\frac{\partial^2 P_3}{\partial t^2}\right)\ . \tag{7}$$

Note that new spatial coordinates ($z_n=nk_x x+k_z z$) have been introduced. These coordinates represent the plane wave character of the solution and allow us to neglect the second spatial and temporal derivatives of the slowly varying envelopes A_n (slowly varying envelope approximation). In this paper we restrict our considerations to the experimentally relevant limit of small angles between the two incident beams, i.e., $k_x/k_z\to 0$. First, the finite value of k_x/k_z is used to split the SBE and the wave equation into a set of equations for the different propagation directions. Once determined we solve this set of equations in the limit $k_x/k_z\to 0$.

The resulting wave equations in the limit of small angles ($k_x/k_z\to 0; z_n=z$) are

$$\frac{\partial\Omega_{-1,1}}{\partial z}+\frac{1}{\omega_L}\frac{\partial\Omega_{-1,1}}{\partial t}=-iKP_{-1,1}\ , \tag{8}$$

$$\frac{\partial\Omega_3}{\partial z}+\frac{1}{\omega_L}\frac{\partial\Omega_3}{\partial t}=-iKP_3\ . \tag{9}$$

Here, the Rabi frequency $\Omega_n = \frac{d \cdot A_n}{\hbar}$ has been introduced as the product of dipole matrix element d and the envelope of the electrical field and $K = 2\mu_0 |d|^2 \omega_L^2 / (a_0^3 \hbar k_z^2)$. The source terms on the right-hand side (RHS) of the propagation equations (8) and (9) are determined by the polarization traveling in the corresponding directions. In principle, we solve the set of equations in infinite order of n. From a simplified point of view, one could say that for the incident pulses $n = -1, 1$ the wave equations are almost the same as for pulse propagation in a single direction, however, the polarizations $P_{-1,1}$ are influenced by the coupling to the FWMS. The incident pulses, $n = \pm 1$, create via the SBE at each sample point a density grating, which diffracts polarization components into the FWM direction. These polarization components in turn create a field which travels through the sample in the FWM direction [see Eq. (9)].

To calculate the polarization components P_n which act as source terms in the different wave equations, a Fourier analysis of the semiconductor Bloch equations has to be carried out. The expansion of the SBE leads to the following general set of equations for the Fourier components:[2,3,9]

$$i\frac{\partial}{\partial t} n^e_{k,n} = \sum_m [\Omega_m]^* P_{k,n-m} - \Omega_m [P_{k,n-m}]^* + \sum_{k'} \nu_{k'} \sum_m [(P_{k+k',m})^* P_{k,n+m} - P_{k+k',n+m} (P_{k,m})^*] \tag{10}$$

and similar for $n^h_{k,n}$,

$$i\frac{\partial}{\partial t} P_{k,n} = \Delta P_{k,n} - \sum_{k'} \nu_{k'} P_{k+k',n} - \sum_m \Omega_m (\delta_{m,n} - n^e_{k,n-m} - n^h_{k,n-m}) \tag{11}$$
$$- \sum_{k'} \nu_{k'} \sum_m [(n^e_{k+k',m} + n^h_{k+k',m}) P_{k,n-m} - (n^e_{k,m} + n^h_{k,m}) P_{k+k',n-m}] \ ,$$

where ν_k is the statically screened Coulomb matrix element. These equations form together with the wave equation a set of partial differential equations of first order. They are solved numerically in infinite order for the characteristic Fourier components with $n = 0, \pm 1, \pm 2, \pm 3$. As usual in pulse propagation studies, the numerical treatment of this system is carried out in a traveling frame:

$$\eta = t - z/\omega_L, \quad \xi = z \ . \tag{12}$$

Since we use reduced wave equations rather than the full Maxwell wave equation, only one boundary condition for each propagation direction has to be fulfilled. At the boundary, Ω_1, Ω_2 are given by the incident pulses. The initial value of the field Ω_3 is zero at the boundary ($z = 0$) for all times. This field is built up inside the sample by the interference of the two incident pulses. All numerical calculations in this paper are carried out for material parameters of GaAs. The dipole moment is 3 eÅ, with e as the electronic charge and the binding energy of the exciton is 4.2 meV.

III. EXCITONIC EFFECTS

In this section we study low-intensity resonant excitation of the $1s$ exciton. We assume Gaussian pulses with 300 fs duration (intensity FWHM) to assure resonant excitation of the $1s$ exciton and no overlap with the continuum states. The phenomenological dephasing time is chosen as 2 ps.

First, we describe the polariton beating at a single resonance system which is in the time domain important to understand low-intensity single pulse propagation as well as propagation effects in the time-resolved and time-integrated FWMS. To illustrate that pulse propagation effects are expected to play an important role in finite samples, Fig. 1 shows the pulse distortion of a Gaussian input pulse after propagation over 1 μm in a GaAs bulk sample. The Gaussian input field amplitude (dashed line) develops a node (solid line) resulting in pulse breakup in the intensity (inset). This feature has been observed experimentally and explained theoretically as the interference of polariton modes.[4] To get a better handle on the analysis of propagation effects in FWMS we discuss the pulse breakup in the time domain. Since we are interested in the origin of the pulse distortion we have additionally plotted in Fig. 1 the polarization source term (short dashed line) which yields the first correction in z to the input field:

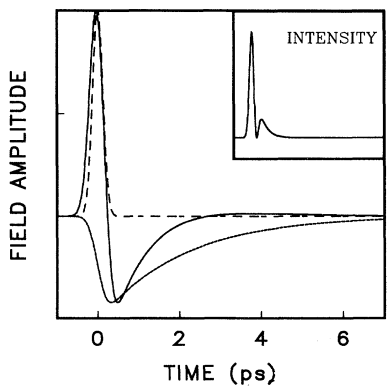

FIG. 1. Field amplitude for incident pulse (medium dashed line), polarization (short dashed line), and resulting field after the propagation (solid line) over 1 μm in GaAs. The inset shows the intensity of the propagated optical field.

$$\Delta A = A_1(t,z) - A_1(t,z=0) = -iK\int_0^z dz' P_1$$
$$\approx -iKzP_1 = -Kz\int_{-\infty}^{t} dt' A_1(t'). \qquad (13)$$

As can be seen in Fig. 1, the imaginary part of the polarization (short dashed) yields for resonant excitation of the exciton a negative contribution after the pulse. According to Eq. (13) the negative polarization leads to an additive negative contribution to the amplitude of the propagating pulse, explaining the development of nodes in the time-dependent pulse intensity after propagation through the sample. For longer samples the number of nodes increases because the distorted field amplitude acts as a source when the field continues to propagate in the sample. Consequently further nodes and peaks occur for further propagation, where the height of the subsequent peaks is always proportional to the area of the respective previous one. Hence, overall the oscillating structure is damped.

With regards to the FWM signal we expect distortions not only because of possible interference and damping effects of the distorted pulses but also because of the nonlinearities in the FWM process itself. To quantitatively study the combined influence of many-body and propagational effects we solve the equations for a sample length $L = 2$ μm. Figure 2 shows the computed time-resolved FWMS for different time delays τ between the incident pulses. We clearly recognize characteristic propagation effects, known from single pulse propagation: The propagation leads to a signal for negative time delays and to time-delayed components, i.e., break up in the time domain. In Ref. 6 similar features in the spectral domain have been reported as a consequence of pulse propagation effects and of exciton-exciton interaction in the local field approximation. In our calculation which contains the full SBE, these results are confirmed if we excite the $1s$ exciton resonance with spectrally sharp pulses. Note that the computed FWMS are modulated with the same frequency dependence which is expected for single propagating pulses (Fig. 1). This behavior may be explained if we imagine that at the beginning of the sample a pulselike FWMS is generated, which then propagates through the sample. We have verified this interpretation by numerically switching off the propagation of the pump pulses after the generation of the FWMS in the first part of the sample. These results obtained for resonant excitation of the exciton within the SBE are similar to recent two-level calculations.[8]

To discuss the length dependence of the propagation effects we now study time-resolved FWMS for different sample lengths between 0 and 4 μm and fixed delay $\tau = 0.3$ ps (see Fig. 3). The figure clearly shows that the signal develops one strong peak which decays into several peaks for increasing propagation length. We observe the strongly peaked signal in the range of 1–2 μm with a maximum around 1.5 μm. This structure can be understood as follows. For short samples the pulse shapes are basically not influenced by propagation since the spatial coupling only enters as a prefactor [Eq. (8)] for the amplitude, i.e., a quadratic length dependence of the FWMS. For longer samples the distortion and therefore interference effects become more important and the simple argument for short samples fails. The propagation-induced interference effects as well as the absorption of the sample result in a decay of the signal after the first local maximum. Figure 3 shows that for longer samples not only the peak value decreases with increasing length, but also the temporal decay of the signal becomes a function of

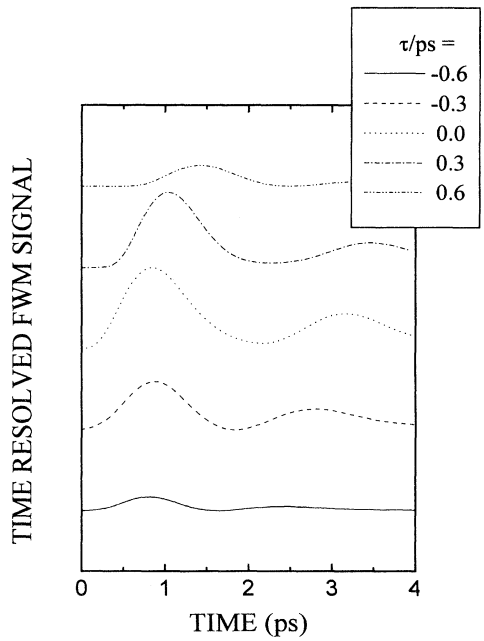

FIG. 2. Time-resolved FWMS for a long sample (2 μm) for different time delays τ. The FWMS shows a similar behavior as a single pulse propagating through the sample. The intensity for the second pulse is 0.015 Rydberg energies (Ry) and for the first, 0.0015 Ry.

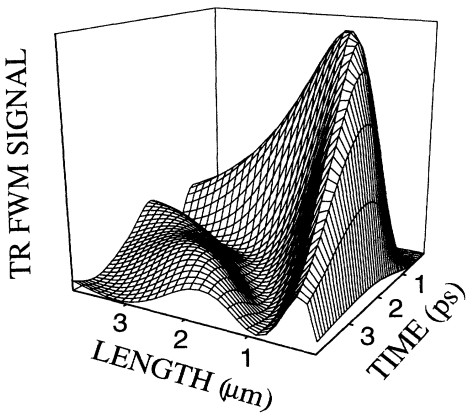

FIG. 3. Time-resolved FWMS (TR FWM signal) at different positions in the sample for a fixed time delay $\tau = 0.3$ ps. Propagation induced modulations develop with increasing sample length. The temporal structure of the FWMS is governed by its own wave equation. Same pulse intensities have been used as in Fig. 2.

the sample length. For samples in excess of 2 μm we see a growth of subsequent peaks in the time domain. Based upon our numerical analysis we can clearly conclude that for longer samples the propagation of the FWMS itself clearly governs the observed signal. Note that after 2 μm an echolike FWM component is built up. This component results from the slightly excited continuum states and is neglected in two-level and local field approaches. A detailed discussion of this signal is given in Sec. V.

In Fig. 4 we show time-resolved signals for the sample lengths 0.07 μm, 0.3 μm, and 0.7 μm. Fitting these curves with an exponential decay we obtain a relaxation time of 0.9 ps for a 0.07μm sample whereas a 0.5 ps decay is observed for a 0.7-μm-thick sample. The original dephasing time of $T_2 = 2$ ps, which is an input parameter in our calculations, marks a limiting value for thin samples as it corresponds to a long time decay proportional to $e^{-(2t)/T_2}$.[1] This behavior shows that even for relatively thin samples the decay time of the real time signal may be different compared to the theoretical limit given by $T_2/2$.

In Appendix A we present the derivation of an approximate formula for the spatial and temporal behavior of the FWMS for long propagation lengths:

$$|\Omega_3|^2 = 49\,\Omega_0^6\,\tau^2\,e^{-2\gamma\tau}\left|\frac{t-\tau}{Kz}\right| J_0^2[2\sqrt{Kz(t-\tau)}] \qquad (t \gtrsim \tau)\ , \quad (14)$$

where Ω_0 is the amplitude of the input pulse. This solution shows that for longer samples the signal develops delayed components and exhibits strong temporal and spatial modulations. To investigate whether experimentally observed modulations are due to propagation effects or coherent dynamics, we suggest in the low-intensity limit the following simple experimental test: First the temporal distortion of a single pulse should be measured. If pulse reshaping effects are in the same order as the modulation of the FWMS, the FWMS is clearly influenced by propagation effects (compare Figs. 1 and 2).

IV. CONTINUUM EFFECTS

In this section we study FWMS for conditions where not only 1s-excitonic but also continuum contributions are relevant. Basically we use the same parameters as for the excitation of the exciton with the exception of a shorter phenomenological dephasing time, $T_2 = 0.5$ ps, for the continuum states. Because of the interaction of the light field with a continuum of states, echolike signals are expected.[3] For excitation inside the continuum we obtain a pure echolike signal at a temporal position close to $2\tau = 2.5$ ps as shown in Fig. 5. The signal increases for the continued propagation through the sample up to a length of 2 μm. After this distance the signal generation process decreases and therefore the absorption becomes more important. The spatial decay of the signal is much weaker than that of the free induction decay due to the smaller spectral weight of the continuum compared with that of the excitonic resonance. No breakup of the echo signal is observed.

A mixture of excitonic and continuum effects is expected for the excitation with a central frequency at the semiconductor band edge because continuum states as well as bound states are excited. Assuming a central frequency of the laser at the band edge and a pulse delay $\tau = 0.3$ ps we obtain the FWM results shown in Fig. 6. For small propagation lengths we see the development of a signal which is more delayed than expected for an echo ($2\tau = 0.6$ ps) and which is asymmetric with respect to its maximum. The asymmetry arises, because we also excite slightly the 1s and the 2s excitonic resonances whose contributions are more delayed than the echolike contribution of the continuum states. Such effects may occur if the dephasing time T_2 is in the order of the time de-

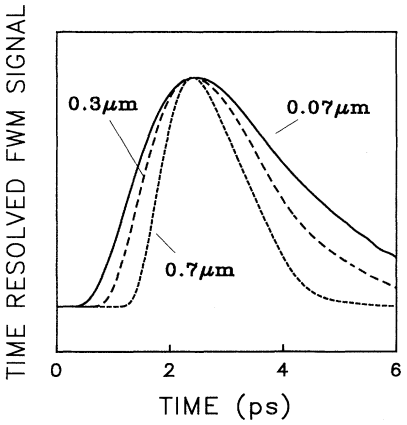

FIG. 4. Time-resolved FWMS for 0.07 μm, 0.3 μm, and 0.7 μm samples. The curves are normalized and shifted so that we obtain the maxima at the same time. The signals are damped due to propagation effects. Same intensities have been used as in Fig. 2.

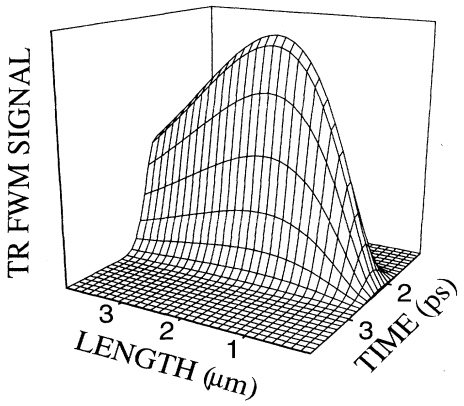

FIG. 5. Time-resolved FWMS calculated for the same parameters as in Fig. 3 and $T_2 = 0.5$ ps. The incident pulses are tuned 3.6 Ry above the band gap for a delay time of $\tau = 1.25$ ps.

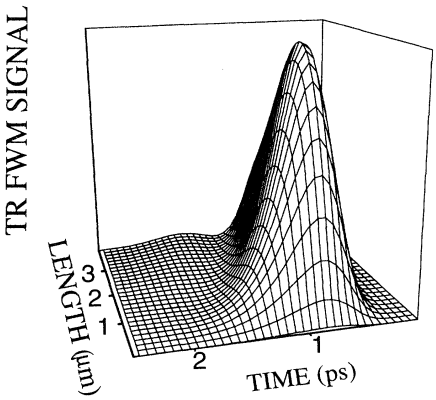

FIG. 6. Time-resolved FWMS calculated for the same parameters as in Fig. 5. The incident pulses are tuned to the band edge and a delay time of $\tau = 0.3$ ps.

lay τ. For increasing propagation length, an increase of the signal amplitude up to 1.6 μm followed by a continuous decay without significant signal modification is observed. With increasing length the signal temporally narrows and becomes more symmetric. In addition to this, a small delayed component occurs. Furthermore, the maximum of the FWMS shifts to smaller times for increased propagation length. The reason for this behavior can be attributed to the different absorption coefficients experienced by the continuum and the excitonic contribution. The excitonic contribution is stronger absorbed than the continuum contribution during their propagation through the sample. For this reason the FWMS develops into a more echolike signal, shifting to smaller times at $2\tau = 0.6$ ps compared to the delayed excitonic contribution.

V. INTENSITY DEPENDENCE

The excitation with low-intensity pulses as discussed in the previous sections shows the basic linear propagation effects of the FWMS but the situation of low excitation does not hold for all experiments. In this section we investigate the intensity dependence of the FWMS for pulses located at the $1s$ resonance. This is not a strong restriction because for sufficiently high intensities, the continuum states shift into resonance with the laser pulse spectrum and become excited as well. Hence, for a certain intensity of the input pulses we expect in general two principal signal contributions for short samples: the free induction decay signal of the excited $1s$ exciton and an excitation-induced component after the second input pulse. Whereas for resonant excitation of the exciton the excitonic signal is generated already at low intensities, the echolike signal originates from the band-gap renormalization, shifting the continuum into resonance with the exciting pulses.[3] The absolute contribution of the excitonic and the continuum part depends on the strength of the band-gap renormalization. For strong excitation the FWMS is dominated by the echolike signal, whereas for low-intensity excitation the excitonic part yields the main contribution.

First, we concentrate on the case where due to a moderate excitation a mixture of the two signal contributions is generated. Our results show the described situation for small sample lengths in Fig. 7. The FWMS develops two peaks at the beginning of the sample: one excitonic and one echolike contribution.[3] Surprisingly, the relative amplitude of both contributions is modified significantly for increasing sample lengths. At the entrance of the sample the excitonic signal dominates whereas after a propagation distance of about 2–3 μm the echo component is predominant. Both components first increase and then develop a maximum which is followed by a decrease. The free induction decay signal of the exciton reaches its maximum at smaller propagation lengths and decays faster than the echo component. At a certain sample length the FWMS only consists of an echolike signal; the excitonic signal has vanished completely. Hence, if the FWMS is detected for a certain sample length, the corresponding signal would suggest Coulomb effects which are different in their absolute strength, depending on which sample length the experiment is carried out.

The analysis shows that our results for increasing propagation distance are easily explained by the different absorption coefficients of exciton and continuum states. For increasing sample lengths the coupling of the polarization and the optical field leads to the increase of the FWMS proportional to its propagation distance. In addition to the generation of the FWMS we have to take into account also the absorption of the signal during its propagation. The different signal components, excitonic and echolike, arising from different parts of the spectrum are differently absorbed during their propagation. Because the free-induction-decay component is mainly absorbed by the excitonic resonance with a relatively high oscillator strength, it is strongly decreased in comparison to the echolike signal. *The shape of the FWMS appears as a result of the dynamic interplay of generation and ab-*

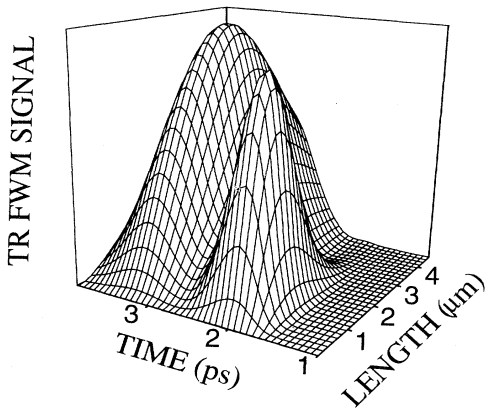

FIG. 7. Time-resolved FWMS calculated for the same parameters as in Fig. 3. The intensity of the incident pulses is increased compared to the parameters of Fig. 3: 0.0175 Ry for the first pulse and 0.035 Ry for the second. The time delay is $\tau = 1.6$ ps.

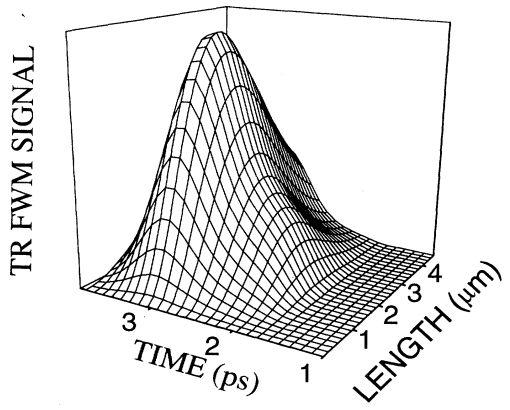

FIG. 8. Time-resolved FWMS calculated for the same parameters as in Fig. 3. The intensity of the first incident pulse is increased compared to the parameters of Fig. 7 up to 0.035 Ry and $\tau = 1.6$ ps.

sorption of the different signal components.

If the input intensity is increased further, a pure echolike signal ($2\tau = 3.2$ ps) is obtained at the beginning of the sample because the continuum states are fully shifted into resonance with the pulse spectrum (Fig. 8). With increasing propagation length, a signal component for earlier times is observed in addition to the echolike component. To appreciate this feature one has to take into account that the input pulses are absorbed while traveling through the semiconductor. For this reason the band-gap renormalization is reduced at longer distances and the input pulses may interact more strongly with excitonic resonances which cause a more significant excitonic contribution to the signal after the second pulse, but before the bulk part of the echo-signal (Fig. 8). This additional signal component occurs before the echolike signal in Fig. 8 ($2\tau = 3.2$ ps).

VI. CONCLUSION

In this paper we have solved the semiconductor Maxwell-Bloch equations for a four-wave-mixing geometry. In the low-intensity regime, we show that the major propagation effects of the FWMS of semiconductors excited at the exciton resonance are due to the propagation of the signal itself, i.e., polariton formation. For resonant excitation of the exciton an approximative expression for the four-wave-mixing signal is given. For higher excitation intensities, where band-gap renormalization occurs, the balance of absorption of the FWMS and generation by the input pulses determines the shape and strength of the signal. In particular, the ratio of excitonic and echolike signal strongly depends on the sample length.

ACKNOWLEDGMENTS

We acknowledge discussions with P. Thomas (Marburg), CPU time from the HLRZ, Jülich, as well as financial support from the DFG through the Sonderforschungsbereich 383.

APPENDIX A

Starting point of our derivation are Eqs. (9) and (B5) including the substitution of the populations with the appropriate polarizations $f_k = |P_k|^2$. This exchange is correct for weak excitations and on the time scale less than the dephasing time. For simplicity, we set the exciton-exciton exchange integral $\beta_1 = 0$. This yields simplified dynamical equations for the $1s$ exciton, including state filling:

$$\frac{\partial}{\partial\eta}P_3 = -i\Omega_3 + i\beta_2 P_1^* P_2 \Omega_2 - \gamma P_3 \ , \tag{A1}$$

$$\frac{\partial}{\partial z}\Omega_3 = -iKP_3 \ , \tag{A2}$$

where $\beta_2 = 7$ characterizes the state filling process of the exciton.

After a Fourier transformation one obtains an equation for the Fourier components of Ω_3:

$$\tilde{\Omega}_3(\omega, z) = \frac{-iK}{i\omega + \gamma}\int_0^z dz' \tilde{Q} e^{\frac{-K}{i\omega+\gamma}(z-z')} \ , \tag{A3}$$

where $\tilde{Q}$ is the Fourier transform of the nonlinear source term in Eq. (A2). Furthermore we use the results of Crisp[12] for the field of single propagating pulses at different propagation distances z.

$$\Omega_1 = \Omega_0 e^{-\frac{\eta}{T_2}}\Theta(\eta) J_0\left(2[Kz\eta]^{\frac{1}{2}}\right) \ , \tag{A4}$$

where Ω_0 is the pulse maximum at $z = 0$. Inserting this known pulse shape into Eq. (A3) the following expression for $\tilde{\Omega}_3$ is obtained:

$$\tilde{\Omega}_3 = \Omega_0^3 \frac{\beta_2}{K} e^{2\gamma\tau}\int_0^z dz' \left(\frac{\partial}{\partial z'} e^{\frac{-K}{i\omega+\gamma}(z-z')}\right)\frac{1}{z'}\int_\tau^\infty d\eta e^{-i\omega\eta} e^{-3\gamma\eta}\sqrt{\eta(\eta-\tau)} \tag{A5}$$

$$\times J_1\left(2[Kz'\eta]^{\frac{1}{2}}\right) J_1\left\{2[Kz'(\eta-\tau)]^{\frac{1}{2}}\right\} J_0\left(2[Kz'(\eta-\tau)]^{\frac{1}{2}}\right) \ ,$$

where τ accounts for the delay time.

Performing a partial integration with respect to z' iteratively we get a series for the FWMS. In the following, we restrict ourselves to contributions close to resonance $\frac{\omega\gamma}{\kappa}\frac{\partial}{\partial z} \to 0$ and develop an approximate solution for large z. Therefore we neglect all terms in higher order of $\frac{1}{z}$ and ω of the expansion of Eq. (A6).

Finally we obtain after a Fourier transformation for the FWMS the asymptotic expression

$$|\Omega_3|^2 = \beta_2^2\,\Omega_0^6\,\tau^2\,e^{-2\gamma\tau}\left|\frac{\eta-\tau}{Kz}\right| J_0^2[2\sqrt{Kz(\eta-\tau)}]. \quad \text{(A6)}$$

Note that this expression is very similar to a single pulse shape, propagating in a resonant medium. This result is in agreement with our numerical calculations.

APPENDIX B

In this appendix we show that with suitably chosen state filling and exchange parameters the simplified equations in the local field approximation yield results which almost quantitatively reproduce the results of the full MSBE as long as we restrict the analysis to excitation at the exciton resonance and relatively low pulse intensities. These approximations have been used successfully to explain several features in semiconductor FWM (Ref. 1) and especially polariton propagation effects in FWM.[6]

Neglecting all contributions except the $1s$-exciton resonance, the semiconductor Bloch equations may be written in the following form:

$$\frac{\partial P}{\partial t} = -i\Omega + i\Delta P + i\beta_2\Omega n + i\beta_1 P n\ , \quad \text{(B1)}$$

$$\frac{\partial n}{\partial t} = i(\Omega^* P - \Omega P^*)\ . \quad \text{(B2)}$$

For GaAs the parameters in the equations are $\beta_1 = 26/3 \times 0.006\,38\ \text{fs}^{-1}$ and $\beta_2 = 7$.[11] The explicit numbers can be obtained by expanding the full SBE in excitonic wave functions. We obtain the polarization on the right-hand side of the Maxwell equation as $P_{\text{tot}} = \frac{2d}{\pi a_0^3}P$. Inserting the Fourier expansions for the polarization and the optical field into polarization and density equation yields

$$\frac{\partial P_{1,-1}}{\partial t} = i\Delta P_{1,-1} - i\Omega_{1,-1}\ , \quad \text{(B3)}$$

$$\frac{\partial n_2}{\partial t} = i(\Omega_1^* P_{-1} - \Omega_{-1}P_1^*)\ , \quad \text{(B4)}$$

$$\frac{\partial P_3}{\partial t} = i\Delta P_3 - i\Omega_3 + i\beta_2\Omega_{-1}n_2 + i\beta_1 P_1 n_2. \quad \text{(B5)}$$

To describe the coupling of the polarization to the electric field, we again use the reduced Maxwell equation with the appropriate Coulomb enhancement factor: $K = 2\mu_0|d|^2\omega_L^2/(\pi a_0^3\hbar k_z^2)$.

The equations for the polarization again form with the wave equations for the corresponding fields a coupled set of partial equations (RE) which has to be solved numerically. The numerical treatment is carried out as described above. Whereas the equations for the components -1 and 1 may now be calculated in a closed form, the FWMS is calculated with the corresponding source terms from the propagation of the pulses in the direction $-1, 1$ and the coupling of the signal itself. To test the quality of Eqs. (B1) and (B2) in comparison to the full MSBE, we show in Fig. 9 the time-resolved FWMS for different propagation lengths. Comparing with the solutions of the full MSBE in Fig. 3 shows good qualitative, almost quantitative agreement indicating that under the carefully chosen conditions we can analyze the FWMS with the numerically less involved reduced equations [Eqs. (B1) and (B2)] (RE) rather than the full MSBE. This calculation confirms the approximations made for the excitation of the $1s$ signal in Ref. 6. Comparing Figs. 9 and 3, the only difference between the reduced and the full calculation is the lack of the small propagation induced echolike signal within the local field model, which can be seen in Fig. 3 after about 2 μm.

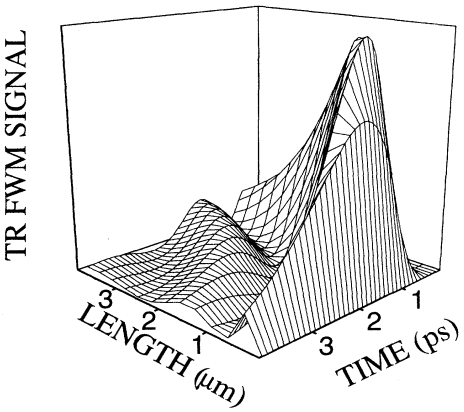

FIG. 9. The time-resolved FWMS has been calculated within the local field approximation for the $1s$ exciton using the same parameters as in Fig. 3. The shape of the FWMS (Fig. 3) is approximately reproduced.

We want to extend our study to time-integrated

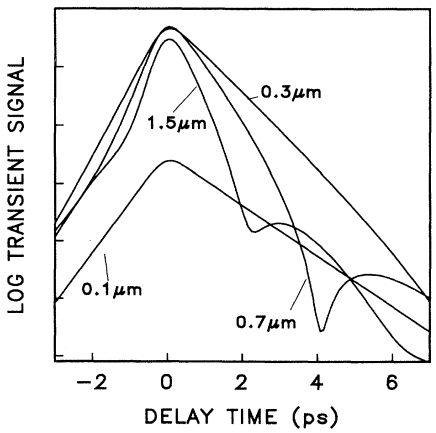

FIG. 10. Transient FWMS including propagation effects for different sample lengths. For numerical convienience, the reduced equations are used.

FWMS. Because of the significant CPU time needed for this we will use the RE. The resulting time-integrated FWMS are shown in Fig. 10. Due to the chosen excitation conditions they are very similar to those obtained in Ref. 6. Whereas the short sample results reproduce the well-known shape dominated by interacting excitons,[1] we obtain for longer samples a substantially faster decay caused by propagation effects. Furthermore, we clearly see a modulation of the time-integrated signal, where the first dip in the curve occurs at the time delay τ of 2 ps. Even though the modulation frequency of the time integrated signal shows the same length dependence as the frequency of the modulations in the real time, it has a different origin. The qualitative structure of the time-resolved FWMS is given by the propagation effects, whereas its height is mostly determined by the overlap of the incident pulses. For small τ there is an overlap at the entrance of the sample and for increasing propagation distances the overlap still exists, because both incident pulses experience basically the same shape modulations. Therefore pulse overlap at each point of the sample contributes to the signal. This situation, however, changes for larger τ. In this case overlap is only generated by the propagation-induced shape modulations after a finite propagation distance. The overlap of different pulse pieces depends strongly on the delay time. Hence, for different τ constructive or destructive interference can be generated and the oscillations in the time-integrated signal for large τ are caused by the resulting interference of the distorted pulses at the end of the sample.

[1] For example, K. Leo, M. Wegener, J. Shah, D. S. Chemla, E. O. Göbel, T. C. Damen, S. Schmitt-Rink, and W. Schäfer, Phys. Rev. Lett. **65**, 1340 (1990); M. Wegener, D. S. Chemla, S. Schmitt-Rink, and W. Schäfer, Phys. Rev. A **42**, 5675 (1990); D. Kim, J. Shah, T. C. Damen, W. Schäfer, F. Jahnke, S. Schmitt-Rink, and K. Köhler, Phys. Rev. Lett. **69**, 2725 (1992); S. Weiss, M.-A. Mycek, J.-Y. Bigot, S. Schmitt-Rink, and D. S. Chemla, *ibid.* **69**, 2685 (1992); H. Wang, K. Ferrio, and D. G. Steel, *ibid.* **71**, 1261 (1993).

[2] For example, see W. Schäfer, F. Jahnke, and S. Schmitt-Rink, Phys. Rev. B **47**, 1217 (1993); H. Wang, K. B. Ferrio, D. G. Steel, P. R. Berman, Y. Z. Hu, R. Binder, and S. W. Koch, Phys. Rev. A **49**, 1551 (1993); Y. Z. Hu, R. Binder, S. W. Koch, S. T. Cundiff, H. Wang, and D. G. Steel, Phys. Rev. B **49**, 14 382 (1994).

[3] M. Lindberg, R. Binder, and S. W. Koch, Phys. Rev. A **45**, 1865 (1992).

[4] D. Fröhlich, A. Kulik, B. Uebbing, A. Mysyrowicz, V. Langer, H. Stolz, and W. von der Osten, Phys. Rev. Lett. **67**, 2343 (1991); D. S. Kim, J. Shah, D. A. B. Miller, T. C. Damen, W. Schäfer, and L. Pfeiffer, Phys. Rev. B **48**, 17 902 (1991).

[5] K. H. Pantke, P. Schillak, B. S. Razbirin, V. G. Lyssenko, and J. M. Hvam, Phys. Rev. Lett. **70**, 327 (1993); P. Schillak and I. Balslev, Phys. Rev. B **48**, 9426 (1993).

[6] T. Rappen, G. Mohs, and M. Wegener, Phys. Rev. B **47**, 9658 (1993); T. Rappen, G. Mohs, and M. Wegener, Phys. Status Solidi B **173**, 77 (1992).

[7] H. Heitz, B. Lummer, J.-M. Wagner, A. Hoffmann, I. Broser, and R. Zimmermann (unpublished).

[8] O. Kinrot and Y. Priop, Phys. Rev. A **50**, 1999 (1994); H. Bakker and H. Kurz, Phys. Rev. B **50**, 7805 (1994).

[9] For a text book discussion see H. Haug and S. W. Koch, *Quantum Theory of the Optical and Electronic Properties of Semiconductors*, 3rd ed. (World Scientific, Singapore, 1994).

[10] W. Schäfer and K. Henneberger, Phys. Status Solidi B **159**, 59 (1990); A. Knorr, R. Binder, M. Lindberg, and S. W. Koch, Phys. Rev. A **46**, 7179 (1992).

[11] L. V. Keldysh and Y. V. Kozlov, Zh. Eksp. Teor. Fiz. **54**, 521 (1968) [Sov. Phys. JETP **54**, 978 (1968)].

[12] M. D. Crisp, Phys. Rev. A **1**, 1604 (1970).